Ground-based transit observations of the HAT-P-18, HAT-P-19, HAT-P-27/WASP40 and WASP-21 systems

M. Seeliger,[1]⋆ M. Kitze,[1] R. Errmann,[1,2] S. Richter,[1] J. M. Ohlert,[3,4] W. P. Chen,[5]
J. K. Guo,[5] E. Göğüş,[6] T. Güver,[7] B. Aydın,[6] S. Mottola,[8] S. Hellmich,[8]
M. Fernandez,[9] F. J. Aceituno,[9] D. Dimitrov,[10] D. Kjurkchieva,[11] E. Jensen,[12]
D. Cohen,[12] E. Kundra,[13] T. Pribulla,[13] M. Vaňko,[13] J. Budaj,[14,13] M. Mallonn,[15]
Z.-Y. Wu,[16] X. Zhou,[16] St. Raetz,[1,17] C. Adam,[1] T. O. B. Schmidt,[1] A. Ide,[1]
M. Mugrauer,[1] L. Marschall,[19] M. Hackstein,[20] R. Chini,[20,21] M. Haas,[20] T. Ak,[7]
E. Güzel,[22] A. Özdönmez,[23] C. Ginski,[1,24] C. Marka,[1] J. G. Schmidt,[1] B. Dincel,[1]
K. Werner,[1] A. Dathe,[1] J. Greif,[1] V. Wolf,[1] S. Buder,[1] A. Pannicke,[1]
D. Puchalski[25] and R. Neuhäuser[1]

[1] *Astrophysical Institute and University Observatory Jena, Schillergäßchen 2-3, D-07745 Jena, Germany*
[2] *Abbe Center of Photonics, Friedrich Schiller Universität, Max-Wien-Platz 1, D-07743 Jena, Germany*
[3] *Astronomie Stiftung Trebur, Michael Adrian Observatorium, Fichtenstraße 7, D-65468 Trebur, Germany*
[4] *University of Applied Sciences, Technische Hochschule Mittelhessen, D-61169 Friedberg, Germany*
[5] *Graduate Institute of Astronomy, National Central University, Jhongli City, Taoyuan County 32001, Taiwan (R.O.C.)*
[6] *Sabanci University, Orhanli-Tuzla 34956, Istanbul, Turkey*
[7] *Faculty of Sciences, Department of Astronomy and Space Sciences, Istanbul University, 34119 İstanbul, Turkey*
[8] *Deutsches Zentrum für Luft- und Raumfahrt e.V., Institut für Planetenforschung, Rutherfordstr. 2, D-12489 Berlin, Germany*
[9] *Instituto de Astrofisica de Andalucia, CSIC, Apdo. 3004, E-18080 Granada, Spain*
[10] *Institute of Astronomy and NAO, Bulgarian Academy of Sciences, 72 Tsarigradsko Chaussee Blvd., 1784 Sofia, Bulgaria*
[11] *Shumen University, 115 Universitetska str., 9700 Shumen, Bulgaria*
[12] *Department of Physics and Astronomy, Swarthmore College, Swarthmore, PA 19081, USA*
[13] *Astronomical Institute, Slovak Academy of Sciences, 059 60, Tatranská Lomnica, Slovakia*
[14] *Research School of Astronomy and Astrophysics, Australian National University, Canberra, ACT 2611, Australia*
[15] *Leibnitz-Institut für Astrophysik Potsdam, An der Sternwarte 16, D-14482 Potsdam, Germany*
[16] *Key Laboratory of Optical Astronomy, NAO, Chinese Academy of Sciences, 20A Datun Road, Beijing 100012, China*
[17] *European Space Agency, ESTEC, SRE-S, Keplerlaan 1, 2201AZ Noordwijk, The Netherlands*
[19] *Gettysburg College Observatory, Department of Physics, 300 North Washington St., Gettysburg, PA 17325, USA*
[20] *Astronomisches Institut, Ruhr-Universität Bochum, Universitätsstraße 150, D-44780 Bochum, Germany*
[21] *Instituto de Astronomía, Universidad Católica del Norte, Avenida Angamos 0610, Casilla 1280 Antofagasta, Chile*
[22] *Faculty of Science, Department of Astronomy and Space Sciences, Univserity of Ege, Bornova, 35100 İzmir, Turkey*
[23] *Graduate School of Science and Engineering, Department of Astronomy and Space Sciences, Istanbul University, 34116 Istanbul, Turkey*
[24] *Sterrewacht Leiden, P.O. Box 9513, Niels Bohrweg 2, 2300RA Leiden, The Netherlands*
[25] *Centre for Astronomy, Faculty of Physics, Astronomy and Informatics, N. Copernicus University, Grudziadzka 5, PL-87-100 Toruń, Poland*

ABSTRACT

As part of our ongoing effort to investigate transit timing variations (TTVs) of known exoplanets, we monitored transits of the four exoplanets HAT-P-18b, HAT-P-19b, HAT-P-27b/WASP-40b and WASP-21b. All of them are suspected to show TTVs due to the known properties of their host systems based on the respective discovery papers. During the past three years 42 transit observations were carried out, mostly using telescopes of the Young Exoplanet Transit Initiative. The analyses are used to refine the systems orbital parameters. In all cases we found no hints for significant TTVs, or changes in the system parameters inclination, fractional stellar radius and planet to star radius ratio and thus could confirm the already published results.

Key words: planets and satellites: individual: HAT-P-18b, HAT-P-19b, HAT-P-27b/WASP-40b, WASP-21b

1 INTRODUCTION

Observing extra solar planets transiting their host stars has become an important tool for planet detection and is used to obtain and constrain fundamental system parameters: The inclination has to be close to $90°$, while the planet to star radius ratio is constrained mainly by the transit depth. Also, in combination with spectroscopy, the semimajor axis and the absolute planet and star radii can be obtained as well.

Several years ago, when the first results of the *Kepler* mission were published (see Borucki et al. 2011 for first scientific results, Koch et al. 2010 for an instrument description), studying the transit timing became one of the standard techniques in the analysis of transit observations. Since space based missions are able to observe many consecutive transit events with a high precision, one can detect even small variations of the transit intervals indicating deviations from a strictly Keplerian motion and thus yet hidden planets in the observed system. Furthermore, with the discovery of multi-planetary systems, transit timing variations (TTVs) are used to find the masses of the companions without the need of radial velocity measurements due to the influence of planetary interaction on TTVs. Since many planet candidates found in photometric surveys are too faint for radial velocity follow-up even with bigger telescopes, TTV analyses can be considered as a photometric work-around to estimate masses.

Although the existence of TTVs can be shown in already known exoplanetary systems, only a few additional planet candidates have been found using TTVs so far (for recent examples of a proposed additional body indicated by TTV analyses see e.g. Maciejewski et al. 2011a and Van Eylen et al. 2014). This is not suprising, since large bodies often can be found using radial velocity measurements or direct transit detections, while small (e.g. Earth-like) objects result in small TTV amplitudes and therefore high precision timing measurements are needed. These measurements can already be acquired with medium size ground-based telescopes.

Commonly the transit mid-time of each observation is plotted into an observed minus calculated (O–C) diagram (Ford & Holman 2007), where the difference between the observed transit mid-time and the mid-time obtained using the initial ephemeris is shown versus the observing epoch. In such a diagram remaining slopes indicate a wrong orbital period, while e.g. periodic deviations from a linear trend indicate perturbing forces.

Besides the discovery of small planets, the amount of known massive planets on close-in orbits increased as well. First studies on a larger sample of planet candidates detected with *Kepler* suggest that hot giant planets exist in single planet systems only (Steffen et al. 2012). However, Szabó et al. (2013) analysed a larger sample of *Kepler* hot Jupiters and found a few cases where TTVs can not be explained by other causes (e.g. artificial sampling effects due to the observing cadence) but the existence of perturbers – additional planets or even exo-moons – in the respective system. In addition Szabó et al. (2013) point toward the planet candidates KOI-338, KOI-94 and KOI-1241 who are all hot Jupiters in multi-planetary systems, as well as the HAT-P-13 system with a hot Jupiter accompanied by a massive planet on an eccentric outer orbit (see also Szabó et al. 2010) and

the WASP-12 system with a proposed companion candidate found by TTV analysis (Maciejewski et al. 2011a).

The origin of those planets is yet not fully understood. One possible formation scenario shows that close-in giant planets could have migrated inwards after their creation further out (Steffen et al. 2012). In that case, inner and close outer planets would have either been thrown out of the system, or caught in resonance. In the latter case, even small perturbing masses, e.g. Earth-mass objects, can result in TTV amplitudes in the order of several minutes (see Ford & Holman 2007 or Seeliger et al. 2014). Though *Kepler* is surveying many of those systems, it is necessary to look at the most promising candidates among all close-in giant planets discovered so far, including stars outside the field of view of *Kepler*. In our ongoing study[1] of TTVs in exoplanetary systems we perform photometric follow-up observations of specific promising transiting planets where additional bodies are expected. The targets are selected by the following criteria:

(i) The orbital solution of the known transiting planet shows non-zero eccentricity (though the circularization timescale is much shorter than the system age) and/or deviant radial velocity (RV) data points – both possibly indicating a perturber.

(ii) The brightness of the host star is $V \leqslant 13$ mag and the transit depth is at least 10 mmag to ensure sufficient photometric and timing precision at 1-2m class ground-based telescopes.

(iii) The target is visible from the Northern hemisphere.

(iv) The target has not been studied for TTV signals before.

In the past the transiting exoplanets WASP-12b (Maciejewski et al. 2011a, 2013b), WASP-3b (Maciejewski et al. 2010, 2013a), WASP-10b (Maciejewski et al. 2011b, Maciejewski et al. 2014 in prep.), WASP-14b (Raetz 2012), TrES-2 (Raetz et al. 2014), and HAT-P-32b (Seeliger et al. 2014) have been studied by our group in detail. In most cases, except for WASP-12b, no TTVs could be confirmed.

Here, we extend our investigations to search for TTVs in the HAT-P-18, HAT-P-19, HAT-P-27/WASP-40 and WASP-21 planetary systems. In Section 2 we give a short description of the targets analysed within this project. Section 3 explains the principles of data acquisition and reduction and gives an overview of the telescopes used for observation. The modeling procedures are described in Section 4, followed by the results in Section 5. Finally, Section 6 gives a summary of our project.

2 TARGETS

2.1 HAT-P-18b and HAT-P-19b

Hartman et al. (2011) reported on the discovery of the exoplanets HAT-P-18b and HAT-P-19b. The two Saturn-mass planets orbit their early K type stars with periods of 5.51d and 4.01d, respectively.

In case of HAT-P-18b Hartman et al. (2011) found the

---

[1] see http://ttv.astri.umk.pl/doku.php for a project overview

Table 1. The observing telescopes that gathered data within the TTV project for HAT-P-18b, HAT-P-19b, HAT-P-27b/WASP-40b and WASP-21b in order of the number of observed transit events of the Observatory. The table lists the telescopes and corresponding observatories, as well as the telescope diameters $\oslash$ and number of observed transit events per telescope in this project N_{tr}.

#	Observatory	Telescope (abbreviation)	$\oslash\,(m)$	N_{tr}
1	Michael Adrian Observatory Trebur (Germany)	T1T (Trebur 1.2m)	1.2	8
2	Graduate Institute of Astronomy Lulin (Taiwan & USA)	Tenagra II (Tenagra 0.8m)	0.8	5
		RCOS16 (Lulin 0.4m)	0.4	2
3	University Observatory Jena (Germany)	90/60 Schmidt (Jena 0.6m)	0.9/0.6	4
		Cassegrain (Jena 0.25m)	0.25	3
4	TÜBİTAK National Observatory (Turkey)	T100 (Antalya 1.0m)	1.0	5
5	Calar Alto Astronomical Observatory (Spain)	1.23m Telescope (CA-DLR 1.2m)	1.23	4
6	Sierra Nevada Observatory (Spain)	Ritchey-Chrétien (OSN 1.5m)	1.5	2
7	Peter van de Kamp Observatory Swarthmore (USA)	RCOS (Swarthmore 0.6m)	0.6	2
8	National Astronomical Observatory Rozhen (Bulgaria)	Ritchey-Chrétien-Coudé (Rozhen 2.0m)	2.0	1
		Cassegrain (Rozhen 0.6m)	0.6	1
9	Teide Observatory, Canarian Islands (Spain)	STELLA-I (Stella 1.2m)	1.2	2
10	University Observatory Bochum (Cerro Armazones, Chile)	VYSOS6 (Chile 0.15m)	0.15	1
11	Xinglong Observing Station (China)	90/60 Schmidt (Xinglong 0.6m)	0.9/0.6	1
12	Gettysburg College Observatory (USA)	Cassegrain (Gettysburg 0.4m)	0.4	1
13	Stará Lesná Observatory (Slovak Rep.)	0.5m Reflector (StaraLesna 0.5m)	0.5	1
14	Istanbul University Telescope at Çanakkale (Turkey)	0.6m Telescope (Çanakkale 0.6m)	0.6	1
15	Toruń Centre for Astronomy (Poland)	0.6m Cassegrain Telescope (Torún 0.6m)	0.6	1

eccentricity to be slightly non-zero ($e = 0.084 \pm 0.048$). Recent studies of Esposito et al. (2014) found the eccentricity to be consistent with a non-eccentric retrograde orbit by analysing the Rossiter-McLaughlin effect. Knutson et al. (2013) also analysed the RV signal and found a jitter in the order of $17.5\,\mathrm{m\,s^{-1}}$ that remains unexplained. Interestingly, the transit data listed in the exoplanet transit database (ETD; Poddaný, Brát, & Pejcha 2010) shows a huge spread in the transit depth in the order of several tens of milli-magnitudes. Thus we included HAT-P-18b in our list of follow-up objects to also confirm or refute these transit depth variations. In addition, we performed a monitoring project for HAT-P-18 over a longer time span to possibly find overall brightness variations. In Ginski et al. (2012) we used lucky imaging with Astralux at the Calar Alto 2.2m Telescope to search for additional low-mass stellar companions in the system. With the data gathered in this previous study we could already exclude objects down to a mass of $0.140 \pm 0.022\,\mathrm{M_\odot}$ at angular separations as small as 0.5 arcsec and objects down to $0.099 \pm 0.008\,\mathrm{M_\odot}$ outside of 2 arcsec.

For HAT-P-19b a small eccentricity of $e = 0.067 \pm 0.042$ was determined by Hartman et al. (2011). They also found a linear trend in the RV residuals pointing towards the existence of a long period perturber in the system. Within this project we want to address the problem of the proposed perturber using photometric methods, i.e. follow-up transit events to find planetary induced TTV signals.

2.2 HAT-P-27b/WASP-40b

HAT-P-27b (Béky et al. 2011), independently discovered as WASP-40b by Anderson et al. (2011) within the WASP-survey (Pollacco et al. 2006), is a typical hot Jupiter with a period of 3.04d. While the eccentricity was found to be $e = 0.078 \pm 0.047$ by Béky et al. (2011), Anderson et al. (2011) adopted a non-eccentric orbit. However, the latter author found a huge spread in the RV data with up to $40\,\mathrm{m\,s^{-1}}$ deviation from the circular single planet solution. According

to Anderson et al. (2011) one possible explanation, despite a changing activity of the K-type host star, is the existence of a perturber that might not be seen in the Béky et al. (2011) data due to the limited data set. However, the authors suggest further monitoring to clearify the nature of the system. One possibility is to study the companion hypothesis from the TTV point of view.

Another interesting aspect of HAT-P-27b is the transit shape which Béky et al. (2011) fitted using a flat bottom model. Anderson et al. (2011) and Sada et al. (2012) found the transit rather to have a roundish shape. From the grazing criterion (Smalley et al. 2011) they concluded that the system is probably grazing, which would explain the unusual shape of the transit. However it is not clear why this is not seen in the Béky et al. (2011) data, hence it is still not clear which shape is real.

2.3 WASP-21b

The planetary host star WASP-21, with its Saturn-mass planet on a 4.32d orbit discovered by Bouchy et al. (2010), is one the most metal-poor planet hosts accompanied by one of the least dense planets discovered by ground-based transit searches to date. Bouchy et al. (2010) found that including a small non-zero eccentricity to the fit does not improve the results. Hence, they concluded that the eccentricity is consistent with zero.

However, in a later study Barros et al. (2011a) found the G3V star to be in the process of moving off the main sequence. Thus, we included further observations of WASP-21b planetary transits to improve the knowledge on this system.

3 DATA ACQUISITION AND REDUCTION

Our observations make use of YETI network telescopes (Young Exoplanet Transit Initiative; Neuhäuser et al. 2011), a worldwide network of small to medium sized telescopes

Table 2. The list of all transit observations gathered within the TTV project sorted by object and date. Though no preselections for quality or completeness have been applied to this list, transits used for further analysis have been marked by an asterisk. The filter subscripts B, C and J denote the photometric systems of Bessel, Cousins and Johnson, respectively. The last column lists the number of exposures and the exposure time of each observation.

#	Date	Telescope	Filter	Exposures
		HAT-P-18b		
1*	2011-04-21	Trebur 1.2m	R_B	189 x 90 s
2	2011-05-02	Trebur 1.2m	R_B	123 x 45 s
3*	2011-05-24	Trebur 1.2m	R_B	323 x 60 s
4	2011-06-04	Rozhen 2.0m	R_C	1000 x 10 s
5*	2012-05-05	Rozhen 0.6m	I_C	219 x 90 s
6	2012-06-07	CA DLR 1.23m	B_J	250 x 60 s
7	2013-04-28	Antalya 1.0m	R	214 x 50 s
8	2014-03-30	Toruń 0.6m	clear	297 x 40 s
		HAT-P-19b		
9*	2011-11-23	Jena 0.6m	R_B	246 x 50 s
10	2011-11-23	Jena 0.25m	R_B	320 x 50 s
11	2011-11-23	Trebur 1.2m	R_B	461 x 30 s
12	2011-12-05	Jena 0.6m	R_B	129 x 60 s
13	2011-12-05	Jena 0.25m	V_B	28 x 300 s
14*	2011-12-09	Jena 0.6m	R_B	290 x 50 s
15	2011-12-09	Jena 0.25m	V_B	118 x 150 s
16	2011-12-09	Trebur 1.2m	R_B	380 x 35 s
17*	2011-12-17	CA DLR 1.23m	R_J	273 x 60 s
18	2014-08-01	Antalya 1.0m	R	148 x 60 s
19	2014-08-05	Antalya 1.0m	R	196 x 40 s
20	2014-08-21	Jena 0.6m	R_B	152 x 50 s
21*	2014-10-04	Jena 0.6m	R_B	280 x 50 s
		HAT-P-27b		
22*	2011-04-05	Lulin 0.4m	R_B	166 x 40 s
23*	2011-04-08	Lulin 0.4m	R_B	250 x 40 s
24	2011-05-03	Stella 1.2m	$H\alpha$	180 x 100 s
25*	2011-05-05	Trebur 1.2m	R_B	162 x 70 s
26	2011-05-08	Stella 1.2m	$H\alpha$	190 x 100 s
27	2011-05-21	Tenagra 0.8m	R	141 x 40 s
28	2012-03-07	StaraLesna 0.5m	R	361 x 30 s
29	2012-03-29	Tenagra 0.8m	R	240 x 30 s
30	2012-04-01	Tenagra 0.8m	R	329 x 20 s
31	2012-04-04	Tenagra 0.8m	R	333 x 20 s
32	2012-04-25	Xinglong 0.6m	R	154 x 40 s
33	2012-05-16	Trebur 1.2m	R_B	231 x 70 s
34	2012-05-25	Chile 0.15m	I_J/R_J	220 x 80 s
35	2012-06-13	Tenagra 0.8m	R	223 x 15 s
36*	2013-06-03	Antalya 1.0m	R	156 x 60 s
37*	2013-06-03	OSN 1.5m	R	435 x 30 s
38	2013-06-06	CA DLR 1.23m	R_J	172 x 60 s
39*	2014-06-18	Antalya 1.0m	R	146 x 50 s
		WASP-21b		
40*	2011-08-24	Swarthmore 0.6m	R_B	545 x 45 s
41	2011-08-24	Gettysburg 0.4m	R	230 x 60 s
42*	2012-08-16	Trebur 1.2m	R_B	365 x 40 s
43	2012-10-20	Antalya 1.0m	R	242 x 40 s
44*	2013-09-18	CA DLR 1.23m	R_J	584 x 30 s
45	2013-09-22	Antalya 1.0m	R	208 x 50 s
46	2013-09-22	Ulupinar 0.6m	R_B	163 x 110 s

mostly on the Northern hemisphere established to explore transiting planets in young open clusters.

A summary of all participating telescopes and the number of performed observations can be found in Table 1. Most of the observing telescopes are part of the YETI network. This includes telescopes at Cerro Armazones (Chile, operated by the University of Bochum), Gettysburg (USA), Jena (Germany), Lulin (Taiwan), Rozhen (Bulgaria), Sierra Nevada (Spain), Stará Lesná (Slovak Republic), Swarthmore (USA), Tenagra (USA, operated by the National Central University of Taiwan) and Xinglong (China). For details about location, mirror and chip see Neuhäuser et al. (2011).

In addition to the contribution of the YETI telescopes, we obtained data using the following telescopes:

• the 1.2m telescope of the German-Spanish Astronomical Center on Calar Alto (Spain), which is operated by German Aerospace Center (DLR).

• the 1.2m robotic telescope STELLA-I, situated at Teide Observatory on Tenerife (Spain) and operated by the Leibniz-Institut für Astrophysik Potsdam (AIP).

• the Trebur 1Meter Telescope operated at the Michael Adrian Observatory Trebur (Germany)

• the T100 telescope of the TÜBITAK National Observatory (Turkey)

• the 0.6m telescope (CIST60) at Ulupınar Observatory operated by Istanbul University (Turkey)

• the 0.6m Cassegrain telescope of the Toruń Centre for Astronomy (Poland)

Besides the transit observations, the Jena 0.6m telescope with its Schmidt Teleskop Kamera (Mugrauer & Berthold 2010) was used to perform a long term monitoring of HAT-P-18 as described in Sections 2.1 and 5.1.

Between 2011 April and 2013 June our group observed 45 transit events (see Table 2) using 18 different telescopes (see Table 1). 15 observations could be used for further analysis, while 30 observations had to be rejected due to several reasons, e.g. no full transit event has been observed or bad weather conditions and hence low signal to noise. E.g. Southworth et al. (2009a,b) showed that defocusing the telescope allows to reduce atmospheric and flat fielding effects. Since a defocused image spreads the light over several CCD pixel, one can increase the exposure time and hence the effective duty cycle of the CCD assuming a constant read out time (as mentioned also in the conclusions of Barros et al. 2011a). Thus we tried to defocuse the telescope and increase the exposure time during all our observations. Table 3 lists the ingress/egress durations τ derived using the formula (18) and (19) given in Winn (2010). With our strategy we obtain at least one data point within 90s. This ensures to have at least 10 data points during ingress/egress phase which is required to fit the transit model to the data and get precise transit mid-times.

All data has been reduced in a standard way by applying dark/bias and flat field corrections using IRAF[2]. The

---

Table 3. The input parameters for the JKTEBOP & TAP runs for all objects listed in Section 2. All values have been obtained from the original discovery papers. LD coefficients are taken from Claret & Bloemen (2011) linear interpolated in terms of T_{eff}, $\log g$ and [Fe/H] using the *EXOFAST/QUADLD* code (Eastman et al. 2013). Free parameters are marked by an asterisk. At the bottom the duration of ingress and egress according to Winn (2010) has been added.

Object	HAT-P-15b	HAT-P-18b	HAT-P-19b	HAT-P-27b	WASP-21b	WASP-38b
$r_{\mathrm{p}} + r_{\mathrm{s}}$*	0.0575(19)	0.0575(19)	0.0709(33)	0.1159(65)	0.0959(44)	0.0829(27)
$R_{\mathrm{p}}/R_{\mathrm{s}}$*	0.1019(09)	0.1365(15)	0.1418(20)	0.1186(31)	0.1040(35)	0.0844(21)
i (°)*	89.1(2)	88.8(3)	88.2(4)	84.7(7)	88.75(84)	89.69(30)
a/R_{s}*	19.16(62)	16.04(75)	12.24(67)	9.65(54)	10.54(48)	12.15(39)
$M_{\mathrm{p}}/M_{\mathrm{s}}$	0.0018(01)	0.000243(26)	0.000329(37)	0.000663(58)	0.000282(19)	0.00213(11)
e	0.190(19)	0.084(48)	0.067(42)	0.078(47)	0	0.0314(46)
P (d)	10.863502(27)	5.5080023(06)	4.008778(06)	3.039586(12)	4.322482(24)	6.871815(45)
R (mag)	11.81	12.61	12.82	11.98	11.52	9.22
T_{eff} (K)	5568(90)	4803(80)	4990(130)	5300(90)	5800(100)	6150(80)
$\log g$ (cgs)	4.38(03)	4.57(04)	4.54(05)	4.51(04)	4.2(1)	4.3(1)
[Fe/H] (dex)	+0.22(08)	+0.10(08)	+0.23(08)	+0.29(10)	-0.46(11)	-0.12(07)
$v \sin i$ (km s^{-1})	2.0(5)	0.5(5)	0.7(5)	0.4(4)	1.5(6)	8.6(4)
LD law of the star	quadratic	quadratic	quadratic	quadratic	quadratic	quadratic
R band linear*	0.4200	0.5736	0.5433	0.4808	0.3228	0.2998
R band non-linear*	0.2525	0.1474	0.1710	0.2128	0.2982	0.3095
V band linear*	0.5274	0.7180	0.6783	0.6002	0.4055	0.3834
V band non-linear*	0.2164	0.0697	0.1039	0.1643	0.2892	0.2992
$\tau_{\mathrm{egress/ingress}}$ (min)	27.8	22.8	23.1	37.8	20.1	21.9

respective calibration images have been obtained in the same night and with the same focus as the scientific observations. This is necessary especially if the pointing of the telescope is not stable. When using calibration images obtained with different foci, patterns remain in the images that lead to distortions in the light curve.

Besides our own observations, we also use literature data. This involves data from the respective discovery papers mentioned in Section 2, as well as data from Esposito et al. (2014) in case of HAT-P-18b, Sada et al. (2012) in case of HAT-P-27b, Barros et al. (2011a) and Ciceri et al. (2013) for WASP-21b, and Simpson et al. (2010) for WASP-38b.

4 ANALYSES

The light curve extraction and modelling is performed analogous to the procedure described in detail in Seeliger et al. (2014).

4.1 Light curve extraction

The Julian date of each image is calculated from the header information of the start of the exposure and the exposure time. To precisely determine the mid-time of the transit event these informations have to be stored most accurate. The reliability of the final light curve model thus also depends on a precise time synchronization of the telescope computer system. Observing transits with multiple telescopes at the same time enables to look for synchronization errors which would otherwise lead to artifacts in the O–C diagram (as shown for HAT-P-27b in epoch 415, see Section 5.3).

We use differential aperture photometry to extract the light curve from the reduced images by measuring the brightness of all bright stars in the field with routines provided by IRAF. The typical aperture radius is $\approx$ 1.5 times the mean full width half maximum of all stars in the field of view (FoV). The best fitting aperture is found by manually varying the aperture radius by a few pixels to minimize the photometric scatter. The final light curve is created by comparing the star of interest against an artificial standard star composed of the (typically 15-30) brightest stars in the FoV weighted by their respective constantness as introduced by Broeg, Fernández, & Neuhäuser (2005).

The final photometric errors are based on the instrumental IRAF measurement errors. The error of the constant comparison stars are rescaled by their photometric scatter using shared scaling factors in order to achieve a mean $\chi^2_{red} \approx 1$ for all comparison stars. The error bars of the transit star are rescaled afterwards using the same scaling factors (for further details on the procedure see Broeg et al. 2005).

Due to atmospheric and air-mass effects transit light curves show trends. They can impact the determination of transit parameters. To eliminate such effects we start the observation about 1 hour before and finish about 1 hour after the transit itself. Thus we can detrend the observations by fitting a second order polynomial to the out-of-transit data.

4.2 Modelling with TAP and JKTEBOP

To model the light curves we used the Transit Analysis Package (TAP; Gazak et al. 2012). The modelling of the transit light curve is done by using the EXOFAST routines (Eastman, Gaudi, & Agol 2013) with the light curve model of Mandel & Agol (2002). For error estimation TAP uses Markov Chain Monte Carlo simulations (in our case 10 times 10^5 MCMC chains) together with wavelet-based likelihood functions (Carter & Winn 2009). The coefficients for the quadratic limb darkening (LD) law used by TAP are taken from the EXOFAST/QUADLD-routine of

Eastman et al. (2013)[3] that linearly interpolates the LD tables of Claret & Bloemen (2011).

For comparison we also use JKTEBOP (see Southworth 2008, and references therein) which is based on the EBOP code for eclipsing binaries (Etzel 1981; Popper & Etzel 1981). To compare the results with those obtained with TAP, we only use a quadratic LD law which is sufficient for ground-based data. For error estimation we used Monte Carlo simulations (10^4 runs), bootstrapping (10^4 data sets), and a residual shift method as provided by JKTEBOP.

As input values we use the system properties presented in the respective discovery papers (see Table 3 for a summary). For both light curve fitting procedures we took the original light curve as well as a threefold binned one. Though the binned light curves result in a lower rms of the fit, no better timing result can be achieved due to a longer cadence.

As free parameters we use the mid-transit time T_{mid}, inclination i, and planet to star radius ratio $k = r_{\mathrm{p}}/r_{\mathrm{S}}$ (with r_{p} and r_{S} being the planet and stellar radius scaled by the semimajor axis, respectively). In case of TAP the inverse fractional stellar radius $a/R_{\mathrm{S}} = 1/r_{\mathrm{S}}$, in case of JKTEBOP the sum of the fractional radii $(r_{\mathrm{p}} + r_{\mathrm{S}})$ is fitted as well. Both quantities are an expression of the transit duration and can be transformed into each other according to the following equation:

$$a/R_{\mathrm{S}} = (1 + r_{\mathrm{p}}/r_{\mathrm{S}}) / (r_{\mathrm{p}} + r_{\mathrm{S}})$$

The fitting procedure is applied two times. First keeping the limb darkening coefficients fixed at their theoretical values, and afterwards letting them vary. For TAP we set the fitting interval to ± 0.2. In case of JKTEBOP we use the option to set the LD coefficients fixed for the initial model, but let them being perturbed for the error estimation. Thus the fitted model does not change, but the error bars are increased. The eccentricity was fixed to zero for all our analyses.

Since all data are obtained using $\mathrm{JD}_{\mathrm{UTC}}$ as time base, we transform the fitted mid-transit times to $\mathrm{BJD}_{\mathrm{TDB}}$ afterwards using the online converter[4] provided by Jason Eastman (for a detailed description of the barycentric dynamical time see Eastman, Siverd, & Gaudi 2010).

Finally, we derive the photometric noise rate (pnr, Fulton et al. 2011) as a quality marker for all light curves, which is defined as the ratio between the root mean square of the model fit and the number of data points per minute. For further analysis we took data with pnr $\lesssim 4.5$ into account.

5   RESULTS

For every light curve we get six different models, four from TAP (for the binned and unbinned data with the LD coefficients fixed and free) and two from JKTEBOP (for the binned and unbinned data, LD coefficients set free for error estimation only). To get one final result we averaged those six results. As for the errors, we got four different estimations from TAP and 12 from JKTEBOP. As final error value, we took the maximum of either the largest of the error estimates, or
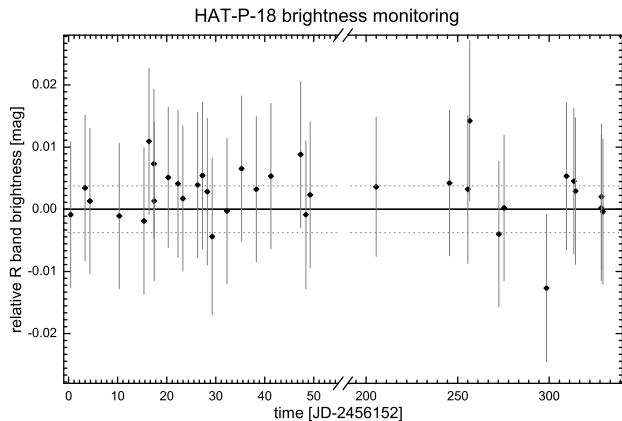

Figure 1. Relative R band brightness of the star HAT-P-18 over a time span of 12 months. The dotted line represents the rms of a constant fit.

the spread of the model fit results to use a conservative error estimate. It has to be noted, though, that the spread between the different models has always been below size of the error bars.

Binning the light curve threefold using an error weighted mean in principle still leaves enough data points during ingress and egress to be able to fit the transit model to the data while reducing the error bar of an individual measurement. However, comparing the results of the threefold binned and unbinned data we do not see significant differences, neither in the fitted values, nor in the error bars.

The same counts for the differences between the TAP models obtained with fixed LD values and those obtained with the LD coefficients set free to fit. For a detailed discussion of the influence of the LD model on transit light curves see e.g. Raetz et al. (2014).

5.1   HAT-P-18b

For HAT-P-18b we obtained five transit light curves (see Fig 2). All light curves show some features which could be caused by stellar activity, e.g. spots. However, the quality of the data does not allow to draw further conclusion. Moreover, there is only a small number of suitable comparison stars available in the respective FoV of each observation, hence this could also be an artificial effect.

Except for one – but not significant – outlier the differences in the O–C diagram (see Fig. 2) can be explained by redetermining the published period by $(0.53 \pm 0.36)\,\mathrm{s}$. Hence we find a slightly larger period compared to the originally proposed period of Hartman et al. (2011).

Regarding the transit depth, and thus the planet to star radius ratio, we do not see any changes. However, having a look at the data provided in the exoplanet transit database (ETD; Poddaný, Brát, & Pejcha 2010) one can see that the values for the transit depth reported there vary by several tens of mmag. Such transit depth variations can be caused by close variable stellar companions placed within the aperture due to the pixel scale of our detectors and the defocussing of the telescopes. Thus we took a more detailed look at

---

[3] the limb darkening calculator is available online at http://astroutils.astronomy.ohio-state.edu/exofast/limbdark.shtml
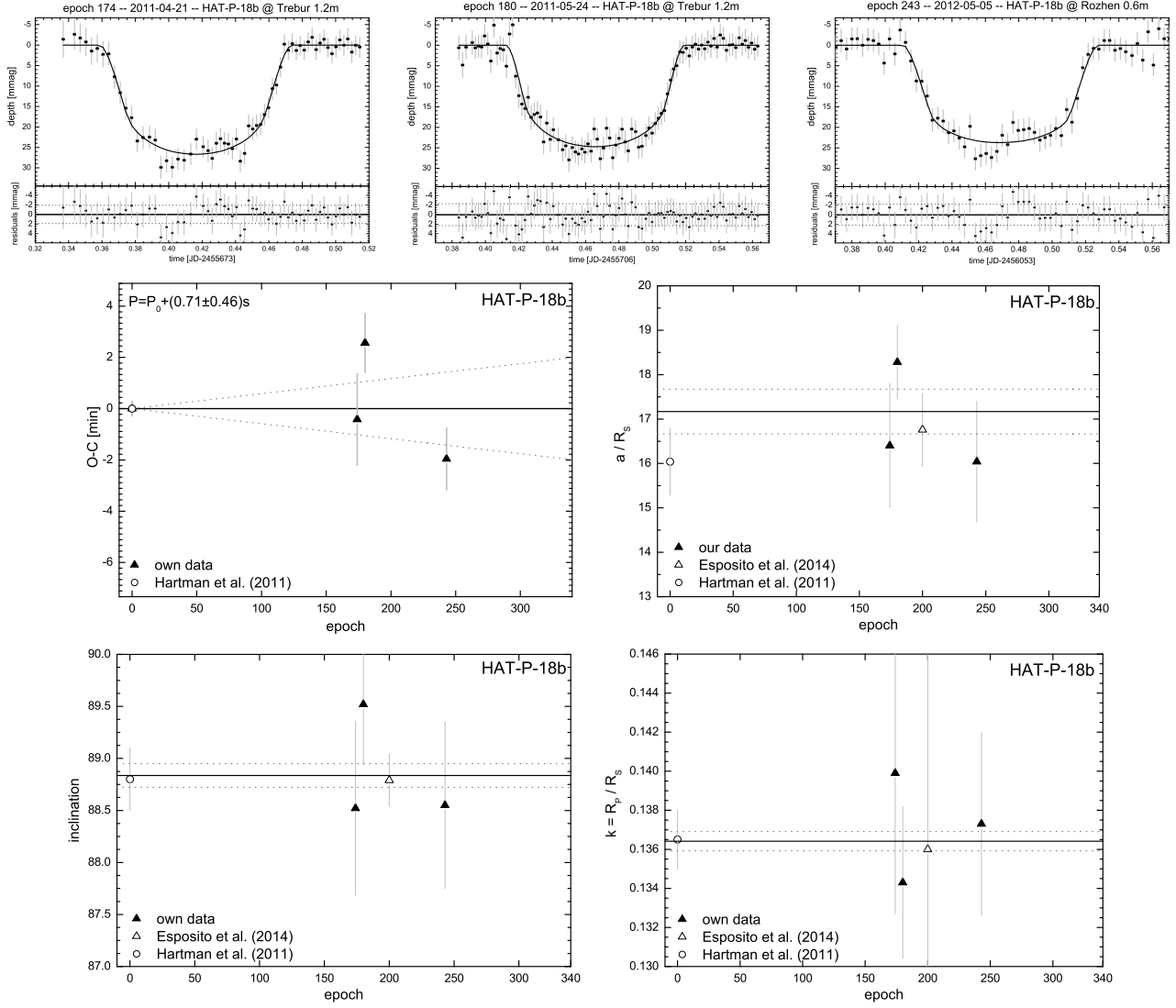[4] http://astroutils.astronomy.ohio-state.edu/time/utc2bjd.html

Figure 2. *top:* The threefold binned transit light curves of the three complete transit observations of HAT-P-18b. The upper panels show the light curve, the lower panels show the residuals. The rms of the fit of the threefold binned light curves (dotted lines) are shown as well. *bottom:* The present result for the HAT-P-18b observing campaign, including the O–C diagram, as well as the results for the reverse fractional stellar radius a/R_S, the inclination i, and the planet to star radius ratio k. The open circle denotes literature data from Hartman et al. (2011), the open triagles denotes data from Esposito et al. (2014). Filled triangles denote our data (from Trebur and Rozhen. The dotted line shows the 1σ error bar of the constant fit.

the long term variability of the parent star. Over a timespan of 12 months we obtained 3 images in four bands (B, V, R, I) in each clear night using the Jena 0.6m telescope. As shown in Fig. 1, the mean variation of the R band brightness is ≈ 3.8 mmag taking the individual error bar of the measurements into account. However, this variation is too small to be responsible for the seen transit depth variations. The monitoring of the remaining bands is not shown but leads to a similar result. Having a closer look at the light curves listed for HAT-P-18b in ETD, one can see that a large number is of lower quality. This is especially true for those light curves responsible for the spread in the tabulated transit depth. Taking only the higher quality data into account the spread is much smaller. Depending on the quality cut the variation can even reach the order of the error bars of the measure-

ments. Thus we believe that the transit depth variation is negligible.

Despite a spread in the data, which can be explained by the quality of the light curves, we do not see any significant difference for k, i and a/R_S between the respective observations. A summary of all obtained parameters can be found in Table 4 at the end of the paper, as well as a comparison with literature values.

5.2 HAT-P-19b

For HAT-P-19b we got two light curves using the Jena 0.6m and one light curve from the CAHA 1.2m telescope (Fig. 3). In all three cases we obtained high precision data. The light curves show no artifacts that could be ascribed to e.g. spots on the stellar surface. Plotting the

mid-transit times into the O–C diagram, we can redetermine the period by (0.53 ± 0.06) s. As for the inclination and the reverse fractional stellar radius we can confirm the values reported in Hartman et al. (2011). The radius ratio of $k = 0.1378 \pm 0.0014$, however, seems to be smaller than assumed by Hartman et al. (2011) ($k = 0.1418 \pm 0.0020$).

5.3 HAT-P-27b

HAT-P-27b planetary transits were observed six times. An advantage of a network such as YETI lies within the possibility of simultaneous observations using different telescopes. This enables us to independently check whether the data is reliable. For HAT-P-27b simultaneous observations could be achieved at epoch 415 using two different telescopes (Antalya 1.0m and OSN 1.5m).

As one can see in Fig. 4 the best-fitting transit shapes differ. Since some data has been acquired using small telescopes under unfavorable conditions, this might be an artificial effect. However, these shape variations can also be seen in the literature data. While Béky et al. (2011) fitted a flat bottom to the transit they observed, the transit of Anderson et al. (2011) shows a rather roundish bottom and so does the Sada et al. (2012) transit. Both Anderson et al. (2011) and Sada et al. (2012) claim, a roundish bottom is in good agreement with a grazing transit. Our most precise transit light curve of HAT-P-27b at epoch 415 the OSN 1.5m telescope also shows no flat bottom. Thus, we would agree with the previous authors that the planet is grazing. The epoch 540 observations also shows a V-shape. However, due to a connection problem parts of the ingress data is missing, thus precise fits of the transit parameters are not possible.

In addition to our own data we added data from Sada et al. (2012) and Brown et al. (2012). The latter one only lists system parameters without giving an epoch of observation, thus we artificially put them to epoch 200. Since we do not see any systematic trend in the remaining data, this does not effect the conclusion on the system parameters but improves the precision of the constant fit.

The system parameters i, a/R_S and k can be determined more precisely than before taking the errors of the individual measurements into account. All three parameters are in good agreement with the results of previous authors. Furthermore, we do not see any significant variation. The larger k-value of the epoch 540 observations are due to the quality of the corresponding light curve.

Looking at the mid-transit time we see that a period change of (-0.51 ± 0.12) s explains the data quite well. The mid-transit time of one of the epoch 415 observations was found to be ≈ 4.5 min ahead of time, while the other one is as predicted. This way we could identify a synchronization error during one of the observations. This example shows the importance of simultaneous transit observations. Unfortunately this was the only sucessful observation of that kind within this project (for a larger set of double and threefold observations see e.g. Seeliger et al. 2014).

5.4 WASP-21b

Four transit light curves of WASP-21b are available, including one light curve from Barros et al. (2011a) (see Fig.5). In addition, the results of the analysis of two transit events of Ciceri et al. (2013) and one transit observation of Southworth (2012) are also taken into account. Concerning the O–C diagram, we found that a period change of (2.63 ± 0.17) s removes the linear trend which is present in the data fitted with the initial ephemeris. As in the previous analyses no trend or sinusoidal variation in the system parameters can be seen.

However, regarding inclination and reverse fractional stellar radius we do see a significant difference between our results and the initial values published by Bouchy et al. (2010). This was also found by other authors before. As discussed in Barros et al. (2011a) this result is a consequence of the assumption of Bouchy et al. (2010) that the planet host star is a main sequence star, while Barros et al. (2011a) found that the star starts evolving off the main sequence and thus its radius increases. This in turn leads to corrections of the stellar and hence planetary properties.

6 SUMMARY

We presented the results of the transit observations of the extra solar planets HAT-P-18b, HAT-P-19b, HAT-P-27b/WASP-40b and WASP-21b which are part of our ongoing project on gound-based follow-up observations of exoplanetary transits using small to medium sized telescopes with the help of YETI network telescopes. During the past three years we followed these well chosen objects to refine their orbital parameters as well as to find transit timing variations indicating yet unknown planetary companions. Table 4 contains an overview of the redetermined properties, as well as the available literature values, while Table 5 lists the results of the individual light curve fits.

In all cases we could redetermine the orbital parameters. Especially the period could be determined more precise than before. So far, we can not rule out the existence of TTV signals for the planets investigated within this study due to the limited number of available high quality data. Also the parameters a/R_S, r_p/r_S and inclination have been obtained and compared to the available literature data. Despite some corrections to the literature data, we found no significant variations within these parameters. To distinguish between a real astrophysical source of the remaining scatter and random noise as a result of the quality of our data more high precision transit observations would be needed.

HAT-P-18b was also part of an out-of-transit monitoring for a spread in the transit depth was reported in the literature that could be due to a significant variability of the transit host star. Regarding our transit data we can not confirm the spread in transit depth. Looking at the quality of the literature data showing the transit depth variation, it is very likely that this spread is of artificial nature. Thus it is not suprising that we did not find stellar variability larger than ≈ 3.8 mmag. However we do see some structures in the light curves that could be caused by spot activity on the stellar surface.
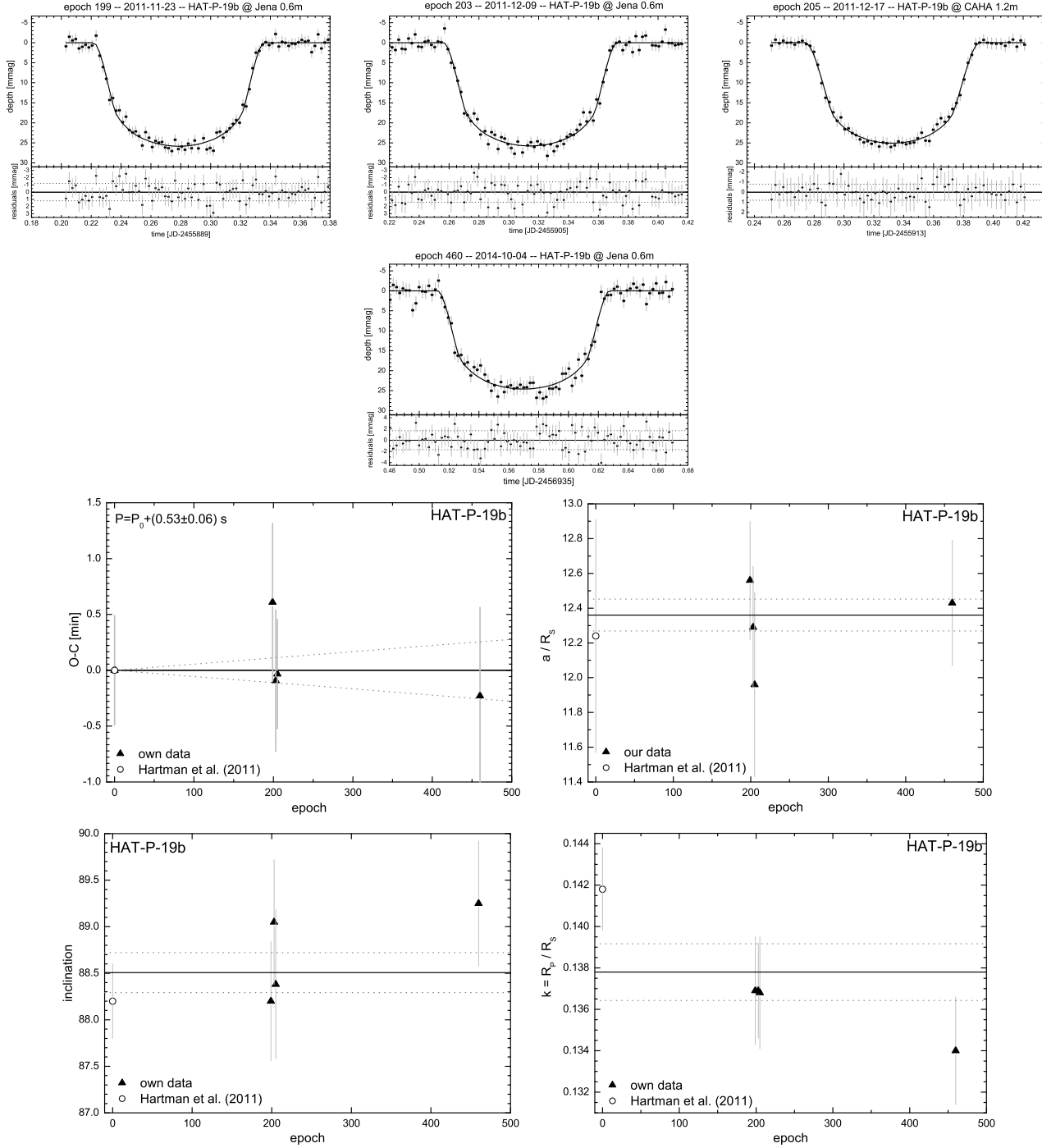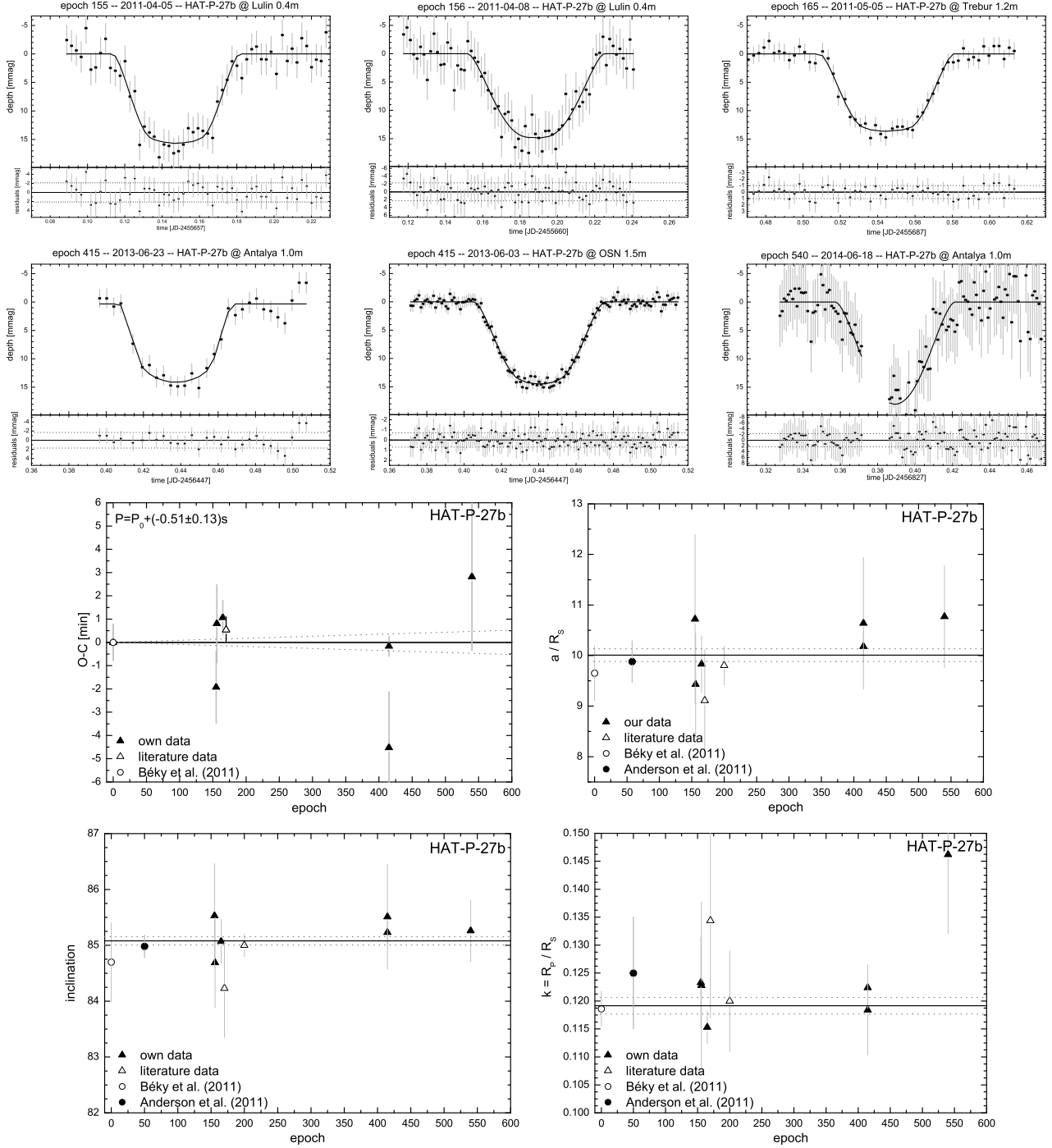
Figure 3. *top:* The transit light curves obtained for HAT-P-19b. *bottom:* The present result for the HAT-P-19b observing campaign. All explanations are equal to Fig. 2. The open circle denotes literature data from Hartman et al. (2011), filled triangles denote our data (from Jena and Calar Alto).

ACKNOWLEDGMENTS

Figure 4. *top:* The transit light curves obtained for HAT-P-27b. *bottom:* The present result for the HAT-P-27b observing campaign. All explanations are equal to Fig. 2. The open circles denotes data from the discovery papers of Béky et al. (2011) and Anderson et al. (2011), open triangles denote literature data from Sada et al. (2012) and Brown et al. (2012) (the latter one set to epoch 200 artificially), filled triangles denote our data (from Lulin, Trebur, Xinglong and Antalya).

Figure 5. *top:* The transit light curves obtained for WASP-21b. *bottom:* The present result for the WASP-21b observing campaign. All explanations are equal to Fig. 2. The open circle denotes data from the discovery paper of Bouchy et al. (2010), open triangles denote literature data from Barros et al. (2011a), Ciceri et al. (2013) and Southworth (2012) (the latter one artificially set to epoch 200), filled triangles denote our data (from Swarthmore, Trebur and Calar Alto).

Table 4. A comparison between the results obtained in Our analysis and the literature data. All epochs T_0 are converted to BJD_{TDB}.

	T_0 (d)	P (d)	$a/R_{\rm s}$	$k = R_{\rm p}/R_{\rm s}$	$i\,(°)$
		HAT-P-18b			
our analysis	$2\,454\,715.022\,54 \pm 0.000\,39$	$5.508\,029\,1 \pm 0.000\,004\,2$	17.09 ± 0.71	$0.136\,2 \pm 0.001\,1$	88.79 ± 0.21
Hartman et al. (2011)	$2\,454\,715.022\,51 \pm 0.000\,20$	$5.508\,023 \pm 0.000\,006$	16.04 ± 0.75	$0.136\,5 \pm 0.001\,5$	88.3 ± 0.3
Esposito et al. (2014)	$2\,455\,706.7 \pm 0.7$	$5.507\,978 \pm 0.000\,043$	16.76 ± 0.82	0.136 ± 0.011	88.79 ± 0.25
		HAT-P-19b			
our analysis	$2\,455\,091.535\,00 \pm 0.000\,15$	$4.008\,784\,2 \pm 0.000\,000\,7$	12.36 ± 0.09	$0.137\,8 \pm 0.001\,4$	88.51 ± 0.22
Hartman et al. (2011)	$2\,455\,091.534\,94 \pm 0.000\,34$	$4.008\,778 \pm 0.000\,006$	12.24 ± 0.67	$0.141\,8 \pm 0.002\,0$	88.2 ± 0.4
		HAT-P-27b			
our analysis	$2\,455\,186.019\,91 \pm 0.000\,44$	$3.039\,580\,3 \pm 0.000\,001\,5$	10.01 ± 0.13	$0.119\,2 \pm 0.001\,5$	85.08 ± 0.07
Béky et al. (2011)	$2\,455\,186.019\,55 \pm 0.000\,54$	$3.039\,486 \pm 0.000\,012$	$9.65^{+0.54}_{-0.40}$	$0.118\,6 \pm 0.003\,1$	$84.7^{+0.7}_{-0.4}$
Anderson et al. (2011)	$2\,455\,368.394\,76 \pm 0.000\,18$	$3.039\,572\,1 \pm 0.000\,007\,8$	9.88 ± 0.39	$0.125\,0 \pm 0.001\,5$	$84.98^{+0.20}_{-0.14}$
Sada et al. (2012)	$2\,455\,186.198\,22 \pm 0.000\,32$	$3.039\,582\,4 \pm 0.000\,003\,5$	$9.11^{+0.71}_{-1.01}$	$0.134\,4^{+0.017\,4}_{-0.038\,9}$	84.23 ± 0.88
Brown et al. (2012)	–	$3.039\,577 \pm 0.000\,006$	$9.80^{+0.38}_{-0.29}$	$0.120^{+0.009}_{-0.007}$	85.0 ± 0.2
		WASP-21b			
our analysis	$2\,454\,743.042\,17 \pm 0.000\,65$	$4.322\,512\,6 \pm 0.000\,002\,2$	9.62 ± 0.17	$0.103\,0 \pm 0.000\,8$	87.12 ± 0.24
Bouchy et al. (2010)	$2\,454\,743.042\,6 \pm 0.002\,2$	$4.322\,482^{+0.000\,024}_{-0.000\,019}$	$6.05^{+0.03}_{-0.04}$	$0.104\,0^{+0.001\,7}_{-0.001\,8}$	$88.75^{+0.70}_{-0.84}$
Barros et al. (2011a)	$2\,455\,084.520\,48 \pm 0.000\,20$	$4.322\,506\,0 \pm 0.000\,003\,1$	$9.68^{+0.30}_{-0.19}$	$0.107\,1^{+0.000\,9}_{-0.000\,8}$	87.34 ± 0.29
Ciceri et al. (2013)	$2\,454\,743.040\,54 \pm 0.000\,71$	$4.322\,518\,6 \pm 0.000\,003\,0$	9.46 ± 0.27	$0.105\,5 \pm 0.002\,3$	86.97 ± 0.33
Southworth (2012)	$2\,455\,084.520\,40 \pm 0.000\,16$	$4.322\,506\,0 \pm 0.000\,003\,1$	9.35 ± 0.34	$0.109\,5 \pm 0.001\,3$	86.77 ± 0.45

Table 5. The results of the induvidual fits of the observed complete transit event. The rms of the fit and the resultant pnr are given in the last column. The table also shows the result for the transits with $pnr > 4.5$ that are not used for redetermining the system properties.

date	epoch	telescope	$T_{\rm mid} - 2\,450\,000$ d	$a/R_{\rm s}$	$k = R_{\rm p}/R_{\rm s}$	$i\,(°)$	rms/pnr (mmag)
			HAT-P-18b				
2011/04/21	174	Trebur 1.2m	$5\,673.419\,67 \pm 0.001\,24$	16.4 ± 1.4	$0.139\,9 \pm 0.007\,2$	88.52 ± 0.84	3.0 / 3.3
2011/05/24	180	Trebur 1.2m	$5\,706.469\,93 \pm 0.000\,80$	18.28 ± 0.83	$0.134\,3 \pm 0.003\,9$	89.52 ± 0.58	3.7 / 4.0
2012/05/05	243	Rozhen 0.6m	$6\,053.472\,76 \pm 0.000\,84$	16.04 ± 1.36	$0.137\,3 \pm 0.004\,7$	88.55 ± 0.79	3.5 / 4.4
2012/06/07	249	CA-DLR 1.2m	$6\,086.518\,56 \pm 0.001\,25$	–	–	–	4.1 / 4.5
2013/04/28	308	Antalya 1.0m	$6\,411.496\,38 \pm 0.000\,84$	15.22 ± 1.52	$0.146\,4 \pm 0.006\,8$	87.89 ± 0.75	3.9 / 5.0
			HAT-P-19b				
2011/11/23	199	Jena 0.6m	$5\,899.283\,45 \pm 0.000\,49$	12.56 ± 0.34	$0.136\,9 \pm 0.002\,6$	88.20 ± 0.64	2.1 / 2.2
2011/12/09	203	Jena 0.6m	$5\,905.318\,10 \pm 0.000\,44$	12.29 ± 0.35	$0.136\,9 \pm 0.002\,3$	89.05 ± 0.67	2.3 / 2.4
2011/12/17	205	CA-DLR 1.2m	$5\,913.335\,71 \pm 0.000\,34$	11.96 ± 0.53	$0.136\,8 \pm 0.002\,7$	88.38 ± 0.80	1.2 / 1.3
2014/10/04	460	Jena 0.6m	$6\,935.575\,59 \pm 0.000\,55$	12.43 ± 0.36	$0.134\,0 \pm 0.002\,6$	89.25 ± 0.67	2.8 / 3.0
			HAT-P-27b				
2011/04/05	155	Lulin 0.4m	$5\,657.153\,33 \pm 0.001\,07$	10.72 ± 1.67	$0.123\,3 \pm 0.008\,1$	85.53 ± 0.93	3.4 / 3.8
2011/04/08	156	Lulin 0.4m	$5\,660.194\,81 \pm 0.001\,16$	9.43 ± 1.01	$0.122\,8 \pm 0.014\,9$	84.69 ± 0.81	3.4 / 3.2
2011/05/05	165	Trebur 1.2m	$5\,687.551\,22 \pm 0.000\,51$	9.83 ± 0.56	$0.115\,3 \pm 0.002\,9$	85.07 ± 0.40	1.6 / 1.8
2012/04/01	274	Tenagra 0.8m	$6\,018.864\,57 \pm 0.002\,32$	9.65 ± 1.63	$0.119\,9 \pm 0.012\,6$	84.13 ± 1.63	5.7 / 5.8
2012/04/25	282	Xinglong 0.6m	$6\,043.180\,95 \pm 0.001\,35$	9.89 ± 1.67	$0.118\,6 \pm 0.006\,7$	84.83 ± 1.24	4.3 / 5.1
2013/06/03	415	Antalya 1.0m	$6\,447.442\,68 \pm 0.001\,66$	10.64 ± 1.30	$0.118\,4 \pm 0.008\,1$	85.51 ± 0.94	2.6 / 3.5
2013/06/03	415	OSN 1.5m	$6\,447.445\,71 \pm 0.000\,30$	10.18 ± 0.29	$0.122\,4 \pm 0.003\,7$	85.23 ± 0.21	1.2 / 0.9
2013/06/18	540	Antalya 1.0m	$6\,827.395\,45 \pm 0.002\,20$	10.77 ± 1.01	$0.146\,2 \pm 0.014\,1$	85.26 ± 0.55	3.1 / 4.0
			WASP-21b				
2011/08/24	244	Swarthmore 0.6m	$5\,797.734\,00 \pm 0.001\,12$	9.94 ± 0.93	$0.101\,4 \pm 0.003\,2$	87.74 ± 1.41	3.3 / 3.1
2012/08/16	327	Trebur 1.2m	$6\,156.502\,60 \pm 0.001\,15$	9.97 ± 0.92	$0.101\,7 \pm 0.003\,2$	87.78 ± 1.46	2.9 / 2.6
2013/09/18	420	CA-DLR 1.2m	$6\,558.496\,48 \pm 0.000\,73$	9.38 ± 0.69	$0.106\,4 \pm 0.002\,7$	86.91 ± 0.96	1.6 / 1.4

References

Adams F. C., Laughlin G., 2006, ApJ, 649, 992

Anderson D. R., et al., 2011, PASP, 123, 555

Bakos G., Noyes R. W., Kovács G., Stanek K. Z., Sasselov D. D., Domsa I., 2004, PASP, 116, 266

Barros S. C. C., Pollacco D. L., Gibson N. P., Howarth I. D., Keenan F. P., Simpson E. K., Skillen I., Steele I. A., 2011b, MNRAS, 416, 2593

Barros S. C. C., et al., 2011a, A&A, 525, A54

Béky B., et al., 2011, ApJ, 734, 109

Borucki W. J., et al., 2011, ApJ, 728, 117

Bouchy F., et al., 2010, A&A, 519, A98

Bodenheimer P., Laughlin G., Lin D. N. C., 2003, ApJ, 592, 555

Broeg C., Fernández M., Neuhäuser R., 2005, AN, 326, 134

Brown D. J. A., et al., 2012, ApJ, 760, 139

Carter J. A., Winn J. N., 2009, ApJ, 704, 51

Ciceri S., et al., 2013, A&A, 557, A30

Claret A., Bloemen S., 2011, A&A, 529, A75

Eastman J., Gaudi B. S., Agol E., 2013, PASP, 125, 83

Eastman J., Siverd R., Gaudi B. S., 2010, PASP, 122, 935

Esposito M., et al., 2014, A&A, 564, L13

Etzel P. B., 1981, in Carling E. B., Kopal Z., eds, Proc. NATO Adv. Study Inst., Photometric and Spectroscopic Binary Systems, Reidel, Dordrecht, p. 111

Ford E. B., Holman M. J., 2007, ApJ, 664, L51

Fulton B. J., Shporer A., Winn J. N., Holman M. J., Pál A., Gazak J. Z., 2011, AJ, 142, 84

Gazak J. Z., Johnson J. A., Tonry J., Dragomir D., Eastman J., Mann A. W., Agol E., 2012, AdAst, 2012, 30

Ginski C., Mugrauer M., Seeliger M., Eisenbeiss T., 2012, MNRAS, 421, 2498

Hartman J. D., et al., 2011, ApJ, 726, 52

Knutson H. A., et al., 2013, arXiv, arXiv:1312.2954

Koch D. G., et al., 2010, ApJ, 713, L79

Kovács G., et al., 2010, ApJ, 724, 866

Maciejewski G., et al., 2010, MNRAS, 407, 2625

Maciejewski G., et al., 2011a, MNRAS, 411, 1204

Maciejewski G., Errmann R., Raetz St., Seeliger M., Spaleniak I., Neuhäuser R., 2011, A&A, 528, A65

Maciejewski G., et al., 2013b, A&A, 551, A108

Maciejewski G., et al., 2013a, AJ, 146, 147

Mandel K., Agol E., 2002, ApJ, 580, L171

Mugrauer M., Berthold T., 2010, AN, 331, 449

Neuhäuser R., et al., 2011, AN, 332, 547

Poddaný S., Brát L., Pejcha O., 2010, NewA, 15, 297

Pollacco D. L., et al., 2006, PASP, 118, 1407

Popper D. M., Etzel P. B., 1981, AJ, 86, 102

Raetz St., 2012, PhD thesis University Jena

Raetz et al., 2014, MNRAS, 444, 1351

Sada P. V., et al., 2012, PASP, 124, 212

Seeliger M., et al., 2014, MNRAS, 441, 304

Simpson E. K., et al., 2010, MNRAS, 405, 1867

Smalley B., et al., 2011, A&A, 526, A130

Southworth J., et al., 2009a, MNRAS, 396, 1023

Southworth J., et al., 2009b, MNRAS, 399, 287

Southworth J., 2008, MNRAS, 386, 1644

Southworth J., 2012, MNRAS, 426, 1291

Steffen J. H., et al., 2012, PNAS, 109, 7982

Szabó G. M., et al., 2010, A&A, 523, A84

Szabó R., Szabó G. M., Dálya G., Simon A. E., Hodosán G., Kiss L. L., 2013, A&A, 553, A17

Van Eylen V., et al., 2014, ApJ, 782, 14

von Essen C., Schröter S., Agol E., Schmitt J. H. M. M., 2013, A&A, 555, A92

Weber M., Granzer T., Strassmeier K. G., 2012, SPIE, 8451,

Winn J. N., 2010, arXiv, arXiv:1001.2010

Wu Z.-Y., Zhou X., Ma J., Jiang Z.-J., Chen J.-S., Wu J.-H., 2007, AJ, 133, 2061